Driving chiral domain walls in antiferromagnets using rotating magnetic fields

Keming Pan,[1] Lingdi Xing,[1] H. Y. Yuan,[2] and Weiwei Wang[1,3,*]
[1]*Department of Physics, Ningbo University, Ningbo 315211, China*
[2]*Department of Physics, Southern University of Science and Technology, Shenzhen 518055, China*
[3]*Institute of Physical Science and Information Technology, Anhui University, Hefei 230601, China*

(Received 6 February 2018; revised manuscript received 25 April 2018; published 15 May 2018)

We show theoretically and numerically that an antiferromagnetic domain wall can be moved by a rotating magnetic field in the presence of Dzyaloshinskii-Moriya interaction (DMI). Two motion modes are found: rigid domain wall motion at low frequency (corresponding to the perfect frequency synchronization) and the oscillating motion at high frequency. In the full synchronized region, the steady velocity of the domain wall is universal, in the sense that it depends only on the frequency of the rotating field and the ratio between DMI strength and exchange constant. The domain wall velocity is independent of the Gilbert damping and the rotating field strength. Moreover, a rotating field in megahertz is sufficient to move the antiferromagnetic domain wall.

DOI: 10.1103/PhysRevB.97.184418

I. INTRODUCTION

Antiferromagnetic spintronics is a rapidly developing research area and has drawn considerable attention recently [1–4]. The antiparallel alignment of the microscopic magnetic moments in antiferromagnets directly leads to two effects. Statically, the net magnetization of antiferromagnets is vanishingly small [3] and thus the antiferromagnetic states are not sensitive to uniform external field. Dynamically, two Landau-Lifshitz-Gilbert equations are needed to describe the dynamics in one unit cell (or equivalently using the coupled equations in terms of the uncompensated magnetization **M** and the Néel order parameter **L** [5–7]), which makes the dynamics of antiferromagnets different from that of ferromagnets. For example, spin waves (magnons) in antiferromagnetic materials provide more degrees of freedom for information encoding [8–10], and the magnonic analog of relativistic Zitterbewegung is predicted in an antiferromagnetic spin chain [11].

Antiferromagnetic domain walls, as another important example, behave differently from the ferromagnetic domain walls. For instance, a static external field failed to move the antiferromagnetic domain walls while it is a well-known force to drive the ferromagnetic domain walls [12]. Antiferromagnetc domain walls (DWs) can be driven by spin waves (magnons) [13–15], external field gradients [16,17], spin-orbit torques [6,7], and thermal gradients [18]. Finding new methods to control the domain wall in antiferromagnets is of great importance.

In this work, we will show that an antiferromagnetic domain wall can be moved by a rotating magnetic field in the presence of Dzyaloshinskii-Moriya interaction (DMI). The DMI is crucial in moving the antiferromagnetic domain walls which is very different from its ferromagnetic counterpart that a rotating magnetic field alone can drive the domain walls effectively [19] without the necessity of DMI. Interestingly, a rotating magnetic field even in megahertz (which is much smaller than the characteristic frequency of an antiferromagnet in terahertz) can move the antiferromagnetc domain walls. The steady velocity of the domain wall only depends on the frequency of the rotating field and is independent of the Gilbert damping and the rotating field strength. Our proposal provides a way to manipulate antiferromagnets.

II. MODEL

We start with a two-sublattice antiferromagnetic (AFM) nanowire along the z axis as illustrated in Fig. 1. The Hamiltonian of the one-dimensional (1D) system is given by [20–22]

$$\mathcal{H} = J\sum_{i}^{2N}\mathbf{S}_i\cdot\mathbf{S}_{i+1} + \sum_{i}^{2N}\mathbf{D}_i\cdot(\mathbf{S}_i\times\mathbf{S}_{i+1}) - K\sum_{i}^{2N}(\mathbf{e}_z\cdot\mathbf{S}_i)^2 - \hbar\gamma\sum_{i}^{2N}\mathbf{H}(t)\cdot\mathbf{S}_i, \quad (1)$$

where $J(>0)$ is the antiferromagnetic exchange constant, $\mathbf{D}_i = D_0\hat{z}$ is the uniform bulk Dzyaloshinskii-Moriya (DM) vector [21,23]. As we will see, the presence of DMI leads to a twisted DW for a head-to-head DW structure. Note that the staggered bulk DMI [23] in the form $\mathcal{H}_{\rm DM} = \mathbf{D}\cdot\sum_i(-1)^i(\mathbf{S}_i\times\mathbf{S}_{i+1})$ does not result in a twisted DW. The uniaxial anisotropy strength is denoted by K and the spin $\mathbf{S}_i$ is treated as a classical vector with length S. The rotating magnetic field $\mathbf{H} = (H\cos\omega t, H\sin\omega t, 0)$ is applied in the xy plane, as shown in Fig. 1.

To proceed, we introduce the net magnetization $\mathbf{m}\equiv(\mathbf{S}_{2i}+\mathbf{S}_{2i-1})/2S$ and the normalized staggered Néel order $\mathbf{n}\equiv(\mathbf{S}_{2i}-\mathbf{S}_{2i-1})/|\mathbf{S}_{2i}-\mathbf{S}_{2i-1}|$ and thus one has $\mathbf{m}\cdot\mathbf{n}=0$ and $\mathbf{n}\cdot\mathbf{n}=1$. In the exchange approximation the Hamiltonian density $\mathcal{H}$ reads [5,16]

$$\mathcal{H} = \frac{1}{2\chi}\mathbf{m}^2 + \frac{A}{2}(\partial_z\mathbf{n})^2 + L\mathbf{m}\cdot\partial_z\mathbf{n} - \frac{K}{2}n_z^2 - \mathbf{m}\cdot\mathbf{h} + D\mathbf{e}_z\cdot(\partial_z\mathbf{n}\times\mathbf{n}), \quad (2)$$

*wangweiwei1@nbu.edu.cn

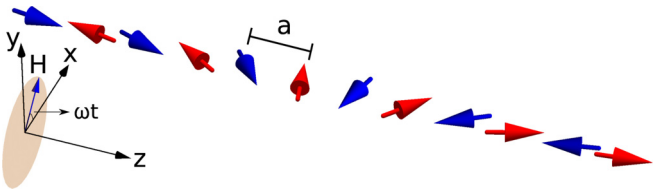

FIG. 1. Illustration of an antiferromagnetic domain wall in an AFM nanowire along the z axis and the nearest-neighbor spacing is a. The rotating magnetic field is applied in the xy plane.

where $\chi^{-1} = 4JS^2/a$ and $A = 2aJS^2$ are homogeneous and inhomogeneous exchange constants with a being the nearest-neighbor spacing in the one-dimensional (1D) system. The L term ($L = 2JS^2$) lifts the energy degeneracy of the sublattice exchange and results in a nonzero magnetization of an antiferromagnetic DW [16]. The anisotropy constant $K = 2K_0S^2/a$, DMI constant $D = D_0S^2$, and the rotating magnetic field $\mathbf{h} = (\hbar\gamma S/a)\mathbf{H}$.

The dynamics of the total magnetization $\mathbf{m}$ and the staggered magnetization $\mathbf{n}$ are given by [13,24]

$$\partial_t \mathbf{n} = -\mathbf{n} \times \mathbf{h}_m, \tag{3a}$$

$$\partial_t \mathbf{m} = -\mathbf{n} \times (\mathbf{h}_n - \alpha \partial_t \mathbf{n}) - \mathbf{m} \times \mathbf{h}_m, \tag{3b}$$

where $\mathbf{h}_m = -\rho^{-1}\delta\mathcal{H}/\delta\mathbf{m}$ and $\mathbf{h}_n = -\rho^{-1}\delta\mathcal{H}/\delta\mathbf{n}$ are effective fields and $\rho = \hbar S/a$ is the density of the staggered spin angular momentum per unit cell [14]. Note that only the phenomenological damping α associated with $\partial_t\mathbf{n}$ is considered. The magnitude of α can be calculated from first-principles calculation [25]. Inserting $\mathbf{h}_m = \rho^{-1}(\mathbf{h} - \mathbf{m}/\chi - L \cdot \partial_z\mathbf{n})$ into Eq. (3), one obtains

$$\chi^{-1}\mathbf{m} = \mathbf{n} \times [(\mathbf{h} \times \mathbf{n}) - \rho\partial_t\mathbf{n}] - L \cdot \partial_z\mathbf{n}, \tag{4}$$

which shows that $\mathbf{m}$ is a slave variable of $\mathbf{n}$.

The static DW profile can be obtained by setting $\partial_t\mathbf{m} = 0$ and $\partial_t\mathbf{n} = 0$ in Eq. (3). Noting that $\mathbf{h}_n = \rho^{-1}(A\partial_{zz}\mathbf{n} + L\partial_z\mathbf{m} + Kn_z\hat{z} - 2D\hat{z} \times \partial_z\mathbf{n})$, in the absence of external field, by eliminating $\mathbf{m}$ we arrive at

$$\mathbf{n} \times [(A - L^2\chi)\partial_{zz}\mathbf{n} + Kn_z\hat{z} - 2D\hat{z} \times \partial_z\mathbf{n}] = 0. \tag{5}$$

Similar to the ferromagnetic case [26], we use the DW ansatz:

$$n_x = \mathrm{sech}[(z-q)/\Delta]\cos[(z-q)\xi + \phi], \tag{6a}$$

$$n_y = \mathrm{sech}[(z-q)/\Delta]\sin[(z-q)\xi + \phi], \tag{6b}$$

$$n_z = -\tanh[(z-q)/\Delta], \tag{6c}$$

where $q = q(t)$ is the DW position, Δ is the domain wall width, $\phi = \phi(t)$ is the DW tilt angle, and ξ is a parameter related to the DMI constant. Substituting Eq. (6) into Eq. (5), we have

$$\xi = \frac{2D}{A}, \quad \Delta = \sqrt{\frac{A}{2K - \xi^2 A}}. \tag{7}$$

For the case $\xi = 0$, the domain wall width reduces to $\Delta_0 = a\sqrt{J/2K_0}$, which is the same as the one in a ferromagnetic spin chain [27]. The presence of external field influences the domain wall profile. For example, a static Zeeman field in the z direction modifies the antiferromagnetic DW width [17].

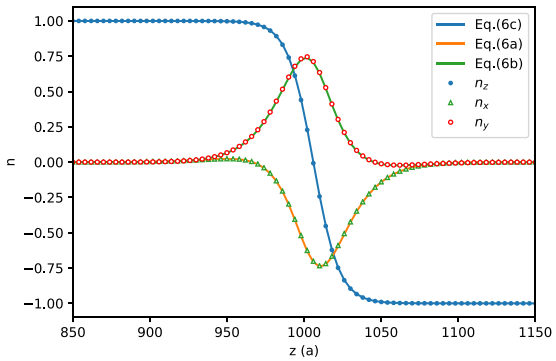

FIG. 2. The domain wall profile obtained by solving the LLG equation. The used simulation parameters are $K_0/J = 0.002$, $D_0/J = 0.02$, and $H/H_0 = 0.004$ with $H_0 = JS/\hbar\gamma$.

In the rotating frame, the rotating field $\mathbf{h}$ is transformed to a static field [28] perpendicular to the z axis. In this situation, the antiferromagnetic DW profile is not sensitive to the static field. Therefore, it is reasonable to use the rigid DW model.

Numerically, the domain wall profile can be obtained by solving the Landau-Lifshitz-Gilbert (LLG) equation

$$\frac{d\mathbf{S}_i}{dt} = -\gamma\mathbf{S}_i \times \mathbf{H}_{\mathrm{eff}} + \frac{\alpha}{S}\mathbf{S}_i \times \frac{d\mathbf{S}_i}{dt}, \tag{8}$$

where α is the Gilbert damping and $\mathbf{H}_{\mathrm{eff}}$ is the effective field given by $\mathbf{H}_{\mathrm{eff}} = -(1/\hbar\gamma)(\partial\mathcal{H}/\partial\mathbf{S}_i)$ with $\gamma(>0)$ the gyromagnetic ratio. Figure 2 shows the domain wall profile [6] using lines. The dots are obtained by solving the LLG equation with the parameters $K_0/J = 0.002$, $D_0/J = 0.02$, and $H/H_0 = 0.004$ with $H_0 = JS/\hbar\gamma$. As we can see, the profile [6] fits the simulation results very well even in the presence of external field applied in the xy plane.

Similar to Eq. (5), the dynamics of DW motion can be obtained by eliminating $\mathbf{m}$:

$$\mathbf{n} \times [-\rho\partial_{tt}\mathbf{n} + T_0 - \chi^{-1}\alpha(\partial_t\mathbf{n}) + T] = 0, \tag{9}$$

where $T_0 = (1/\rho\chi)[(A/2)\partial_{zz}\mathbf{n} + Kn_z\hat{z} - 2D\hat{z} \times \partial_z\mathbf{n}]$ and $T = 2\mathbf{h} \times \partial_t\mathbf{n} - \rho^{-1}(\mathbf{n} \cdot \mathbf{h})\mathbf{h} - L\partial_z\mathbf{n} \times \partial_t\mathbf{n} + \partial_t\mathbf{h} \times \mathbf{n}$. Here, we assume that the domain wall structure is rigid and thus use two parameters [the DW position $q = q(t)$ and the DW tilt angle $\phi = \phi(t)$] to describe the domain wall dynamics. Applying the collective coordinate approach [5], we have $\partial_t\mathbf{n} = \dot{\phi}\partial_\phi\mathbf{n} + \dot{q}\partial_q\mathbf{n}$ and $\partial_{tt}\mathbf{n} = \ddot{\phi}\partial_\phi\mathbf{n} + \ddot{q}\partial_q\mathbf{n} + \dot{\phi}^2\partial_{\phi\phi}\mathbf{n} + \dot{q}^2\partial_{qq}\mathbf{n} + 2\dot{\phi}\dot{q}\partial_{\phi q}\mathbf{n}$ where the overdot represents $\partial/\partial t$. For the domain wall profile (6), one has $\partial_q\mathbf{n} = -\partial_z\mathbf{n}$ and $\partial_\phi\mathbf{n} = \hat{z} \times \mathbf{n}$. Applying the cross product of $\partial_q\mathbf{n}$ (and $\partial_\phi\mathbf{n}$) to Eq. (9) and integrating over the whole nanowire region, we have

$$\left(\frac{\alpha}{\chi}\dot{Q} + \rho\ddot{Q}\right) - \frac{\kappa\Delta}{1+\kappa^2}\left(\frac{\alpha}{\chi}\dot{\psi} + \rho\ddot{\psi}\right) = c\Delta\dot{\psi}\cos\psi \tag{10a}$$

$$\left(\frac{\alpha}{\chi}\dot{Q} + \rho\ddot{Q}\right)\kappa - \left(\frac{\alpha}{\chi}\dot{\psi} + \rho\ddot{\psi}\right)\Delta - \frac{\alpha}{\chi}\frac{\omega\Delta}{1+\kappa^2} = (1+\kappa^2)c\dot{Q}\cos\psi + d\Delta\sin 2\psi, \tag{10b}$$

where $c = (1/2)h_0\pi\,\mathrm{sech}(\pi\kappa/2)$, $d = (1/2\rho)h_0^2\pi\kappa\,\mathrm{csch}(\pi\kappa)$, and $\kappa = \xi\Delta$. Also, we have introduced $\psi = \phi - \omega t$ and $Q = q - \omega\kappa\Delta t/(1+\kappa^2)$.

III. RESULTS

Equation (10) is a coupled second-order differential equation. Here, we show that Eq. (10) has a special solution:

$$\dot{Q} = 0, \quad \dot{\psi} = 0, \quad \sin 2\psi = -\frac{\alpha}{\chi}\frac{\omega}{d(1+\kappa^2)}. \tag{11}$$

It is straightforward to see that $\dot{\psi} = 0$ gives $\dot{\phi} = \omega$, which corresponds to the perfect frequency synchronization. In this scenario, the angular velocity of the DW rotation is exactly the same as the frequency of the rotating field. The steady velocity of DW is

$$v = \dot{q} = \frac{\omega\kappa\Delta}{1+\kappa^2}. \tag{12}$$

The velocity, Eq. (12), scales linearly with the frequency ω of the rotation field. The presence of DMI is critical in driving the antiferromagnetic domain wall since a nonzero velocity requires that $\kappa \neq 0$. Without the DMI, the velocity of the antiferromagnetic DW is zero, which is different from the ferromagnetic case that a rotating field alone can drive the ferromagnetic DW motion [19]. For the ferromagnetic case, a head-to-head DW and a tail-to-tail DW move in opposite directions when driven using rotating fields. The antiferromagnetic DW can be considered as a combination of a head-to-head DW and a tail-to-tail DW and thus the antiferromagnetic DW velocity is zero. In the presence of DMI the DW becomes twisted, which induced a symmetry breaking. In this scenario the two twisted ferromagnetic DWs failed to cancel each other totally and thus results in a net velocity. Moreover, the DW angle rotates with an angular velocity of ω due to the synchronization of rotation field. Interestingly, the velocity [Eq. (12)] is independent from the Gilbert damping α and the strength of the rotational field, which is because the motion of DW in the presence of DMI can be considered as a side effect of the frequency synchronization.

Using Eq. (11), the critical frequency ω_c can be found as

$$\omega_c = \frac{\chi}{\alpha}(1+\kappa^2)d. \tag{13}$$

As can be seen, the critical frequency ω_c is proportional to the square of the external field strength, and a larger damping α leads to a smaller ω_c.

The perfect synchronized motion is valid only in the region $\omega < \omega_c$. For the case that the frequency is larger than the critical frequency ($\omega > \omega_c$), an oscillation motion emerges. By using the assumption

$$\frac{d\psi}{dt} = -g(\omega + \omega_c)\sin 2\psi, \tag{14}$$

where g is a parameter related to rotating field, one finds that (see Appendix B for details)

$$\langle dQ/d\psi\rangle = \frac{\Delta\kappa}{1+\kappa^2}. \tag{15}$$

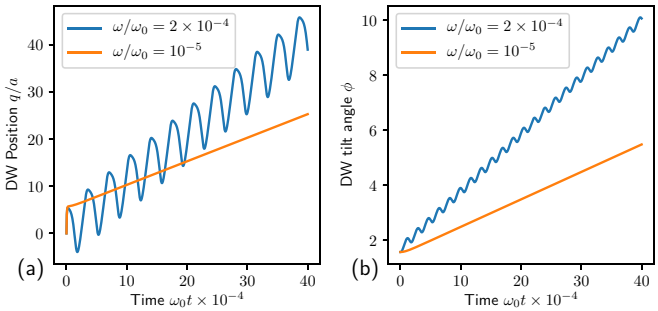

FIG. 3. (a) The DW position as a function of time for $\omega/\omega_0 = 10^{-5}$ and $\omega/\omega_0 = 2\times10^{-4}$. (b) The DW tilt angle as a function of time for $\omega/\omega_0 = 10^{-5}$ and $\omega/\omega_0 = 2\times10^{-4}$. The dimensionless time 10 corresponds to approximately 40 ns for $KMnF_3$. The data is obtained by solving the LLG equation numerically. The used simulation parameters are $H/H_0 = 5\times10^{-4}$, $\alpha = 5\times10^{-4}$, $D_0/J = 0.02$, and $K_0/J = 0.002$.

Using Eq. (14), the solution of ψ can be found as

$$\tan\psi = -\frac{\omega_c}{\omega} - \sqrt{1-\left(\frac{\omega_c}{\omega}\right)^2}\tan\left(gt\sqrt{\omega^2-\omega_c^2} - \psi_0\right). \tag{16}$$

The period is $T = \pi/(g\sqrt{\omega^2-\omega_c^2})$ and thus the average $\dot{\psi}$ can be computed as $\langle\dot{\psi}\rangle = -g\sqrt{w^2-\omega_c^2}$. Therefore, we obtain the average velocity for $\omega > \omega_c$:

$$\langle\dot{q}\rangle = \frac{\Delta\kappa}{1+\kappa^2}\left(\omega - g\sqrt{w^2-\omega_c^2}\right), \tag{17}$$

where g is given by Eq. (B7).

To verify our analytical results for the two scenarios, we perform numerical simulations based on the LLG equation (8) and the Hamiltonian (1). In practice, it is convenient to use the dimensionless LLG equation (see Appendix A). As shown in Appendix A, the dimensionless LLG equation can be characterized by several parameters: the damping α, the dimensionless time $t' = (JS/\hbar)t$, the dimensionless external field $(\hbar\gamma/JS)H$, and the energy ratios D_0/J and K_0/J. Therefore, we introduce a characteristic frequency $\omega_0 = JS/\hbar$ and a characteristic field $H_0 = \omega_0/\gamma$. For $KMnF_3$, the typical parameters are $a = 0.418$ nm, $S = 5/2$, and $J = 0.656$ meV [29,30], which results in $\omega_0 = 2.48\times10^3$ GHz and $H_0 = 14.14$ T. Also, evidence of nonzero DMI in $KMnF_3$ is reported [31].

Figure 3(a) shows the DW position as a function of time for the cases $\omega/\omega_0 = 10^{-5}$ and $\omega/\omega_0 = 2\times10^{-4}$ where the parameters $H/H_0 = 5\times10^{-4}$, $\alpha = 5\times10^{-4}$, $D_0/J = 0.02$, and $K_0/J = 0.002$ are used. It can be found that for the low frequency case ($\omega/\omega_0 = 10^{-5}$) the DW displacement is a linear function of time, as predicted by Eq. (12). The corresponding DW tilt angle ϕ is shown in Fig. 3(b). We conclude that the low frequency case ($\omega/\omega_0 = 10^{-5}$) corresponds to the perfect synchronized motion because the rotation frequency of DW plane $\langle\dot{\phi}\rangle$ is equal to the frequency of the rotation wave. For the high frequency case ($\omega/\omega_0 = 2\times10^{-4}$), the DW moves back and forth, corresponding to the incomplete synchronized region. In this region, the DW tilt angle also shows an oscillation and the rotation frequency of DW plane

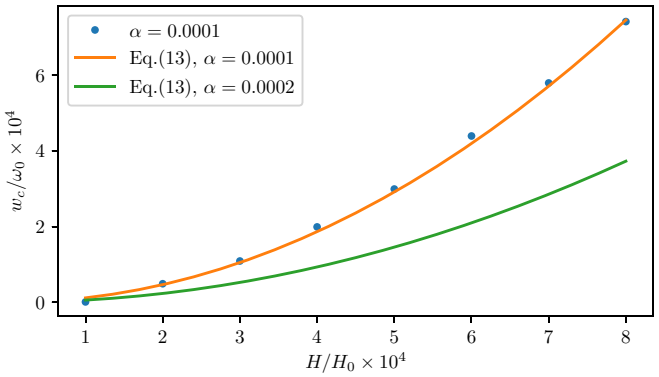

FIG. 4. The critical frequency ω_c as a function of the rotating field strength. The dots are obtained using numerical simulation. The lines are plotted using Eq. (13). The dimensionless field strength 5.0 corresponds to 7.07 mT while the dimensionless frequency 4.0 corresponds to 0.99 GHz for $KMnF_3$.

$\langle\dot{\phi}\rangle$ is smaller than the rotating field frequency ω, as depicted in Fig. 3(b).

To get further insight into the magnitude of critical frequency ω_c, we plot ω_c as a function of the rotating field strength in Fig. 4. The dots are obtained by solving the LLG equation directly and the lines are plotted using Eq. (13); it is found that the analytical result, Eq. (13), agrees with the simulation results very well. For $KMnF_3$, the used frequency is in megahertz ($\omega/\omega_0 = 10^{-5}$ corresponds to $\omega = 24.8$ MHz). The amplitude of the rotating field is $H = 7$ mT for $H/H_0 = 5 \times 10^{-4}$. Therefore, a rotating field in the megahertz frequency range is sufficient to move the chiral antiferromagnetic DW motion.

Figure 5 plots the DW velocity as a function of the rotating field frequency where the dots are obtained using numerical simulations while the lines are plotted analytically [Eq. (12) for $\omega < \omega_c$ and Eq. (17) for $\omega > \omega_c$]. In the region $\omega < \omega_c$ the DW

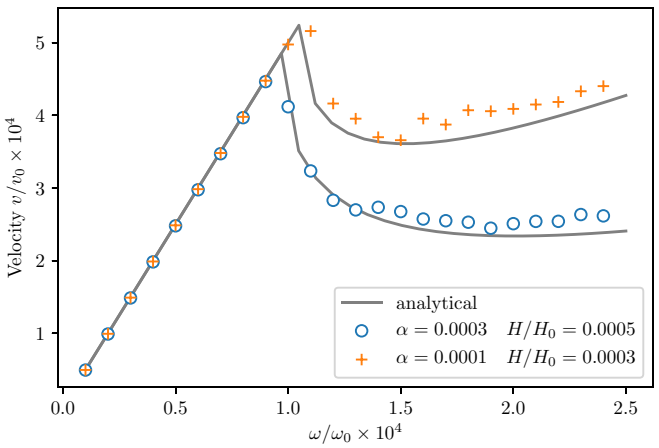

FIG. 5. The (average) DW velocity as a function of the rotating field frequency obtained by numerical simulations with parameters (i) $\alpha = 0.0003$ and $H/H_0 = 0.0005$, and (ii) $\alpha = 0.0001$ and $H/H_0 = 0.0003$. Gray lines are plotted using analytical equations (12) and (17). The dimensionless frequency 1.0 corresponds to 0.25 GHz while the dimensionless velocity 1.0 corresponds to 0.1 m/s for $KMnF_3$.

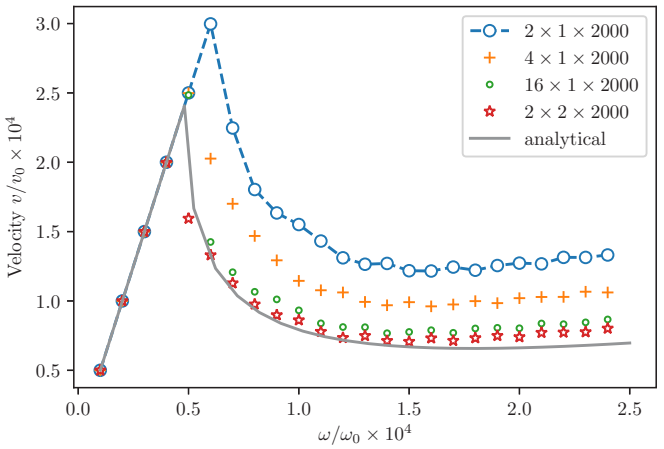

FIG. 6. The DW velocity as a function of the rotating field frequency for the 2D/3D system. The parameters used in simulations are $\alpha = 0.0003$ and $H/H_0 = 0.0005$.

velocity agrees with analytical prediction very well. We have introduced a characteristic velocity $v_0 = \omega_0 a$. For $KMnF_3$, $v_0 = 1.04 \times 10^3$ m/s. So the typical velocity is 0.5 m/s. This speed is smaller than the typical speed driven by the spin waves [13] and spin-orbit torques [6]. Also, it can be seen that the velocity is universal in the region $\omega < \omega_c$ since different parameters result in the same velocity. In the region $\omega > \omega_c$, there is a small deviation between the analytical result, Eq. (17), and the numerical simulations, which is because Eq. (14) is not an exact solution of coupled differential equation (10).

It is interesting to ask whether the critical frequency ω_c obtained by Eq. (13) is reasonable for a two- (2D) or three- (3D) dimensional system. The number of nearest neighbors N_D for the squared (2D) and simple cubic (3D) lattice are $N_D = 4$ and $N_D = 6$, respectively. Therefore, we have $\rho = 2\hbar S/V$ (the density of the staggered spin angular momentum per unit cell), $\chi^{-1} = 4N_D J S^2/V$, and $\mathbf{h} = (2\hbar\gamma S/V)\mathbf{H}$ where V is the volume of the unit cell and $V = 2a$ for the 1D unit cell and $V = 2a^2$ for the 2D unit cell. By analyzing the Eq. (13), we find

$$\omega_c = \frac{2}{N_D}\omega_c^{1D} \tag{18}$$

and thus $\omega_c^{2D} = (1/2)\omega_c^{1D}$ and $\omega_c^{3D} = (1/3)\omega_c^{1D}$ due to the fact that for 2D or 3D systems each spin has more nearest neighbors.

Figure 6 shows the DW velocity as a function of the rotating field frequency for the 2D/3D system with different sizes and the parameters $\alpha = 0.0003$ and $H/H_0 = 0.0005$ are fixed in the simulation. Similar to the 1D system, in the low frequency region the DW velocity increases linearly as the frequency increases. In the high frequency region, the DW speed shows a Walker breakdown. The critical frequency for the 1D system is $\omega_c/\omega_0 \approx 10^{-4}$ and thus the predicted critical frequency for 2D is $\omega_c^{2D}/\omega_0 \approx 0.5 \times 10^{-4}$. As the system size increases, it can be seen that the critical frequency is converged to the predicted one. Moreover, the velocity also approaches the analytical result for the 2D system as plotted in Fig. 6 using a gray line. A 3D system with size $2 \times 2 \times 2000$ is presented in Fig. 6 as well; the velocity for this quasi-1D system is similar to that obtained using bulk DMI.

IV. SUMMARY

In summary, we have studied the antiferromagnetic domain wall motion driven by a rotating field in the presence of Dzyaloshinskii-Moriya interaction. We found that the DMI is critical in moving the antiferromagnetic DW. Two DW motion modes are found: in the low frequency region, the DW performs a perfect synchronized motion with the rotational field. The steady domain wall velocity is only related to the frequency of the rotating field as well as the strength of DMI and it is independent of the Gilbert damping and the rotating field strength. In the high frequency region (which corresponds to the incomplete synchronized region), the domain wall shows a ratchet motion.

ACKNOWLEDGMENTS

We acknowledge the financial support from National Natural Science Foundation of China (Grants No. 11604169 and No. 61704071).

APPENDIX A

The effective field at site i is given by $\mathbf{H}_i = -(1/\hbar\gamma)[J(\mathbf{S}_{i-1}+\mathbf{S}_{i+1}) + \mathbf{D}\times(\mathbf{S}_{i-1}-\mathbf{S}_{i+1}) - 2K_0(\mathbf{e}_z\cdot\mathbf{S}_i)\mathbf{e}_z - \hbar\gamma\mathbf{H}]$. Inserting the effective field into the LLG equation (8), we have

$$\frac{d\mathbf{u}_i}{dt'} = \alpha\mathbf{u}_i\times\frac{d\mathbf{u}_i}{dt'} - \mathbf{u}_i\times[(\mathbf{u}_{i-1}+\mathbf{u}_{i+1}) - 2(K_0/J)u_i^z\hat{z} + (D_0/J)\hat{z}\times(\mathbf{u}_{i-1}-\mathbf{u}_{i+1}) - (\hbar\gamma/JS)\mathbf{H}], \quad \text{(A1)}$$

where $\mathbf{u}_i = \mathbf{S}_i/S$ is the unit vector of $\mathbf{S}_i$ and $t' = (JS/\hbar)t$ (the time t is in SI units). From the dimensionless equation (A1), we conclude that the system which is governed by the LLG equation (8) and the associated Hamiltonian (1) can be characterized by several parameters: the damping α, the ratios D_0/J and K_0/J, and the rotating field $(\hbar\gamma/JS)\mathbf{H}$.

APPENDIX B

The variable Q can be considered as a function of ψ, i.e., $Q = Q(\psi)$, so we have $\dot{Q} = \dot{\psi}Q' = YQ'$ where $Y = \dot{\psi}$ and $'$ represents the derivative with respect to ψ. Notice that when $\ddot{Q} = \dot{\psi}^2Q'' + \ddot{\psi}Q'$ and $\ddot{\psi} = \dot{Y} = YY'$, we have

$$X - \frac{\kappa\Delta}{1+\kappa^2}\left(\frac{\alpha}{\chi}+\rho Y'\right) = c\Delta\cos\psi, \quad \text{(B1)}$$

$$XY\kappa - \left(\frac{\alpha}{\chi}Y+\rho Y'\right)Y\Delta - \frac{\alpha}{\chi}\frac{\omega\Delta}{1+\kappa^2} = (1+\kappa^2)cYQ'\cos\psi + d\Delta\sin 2\psi, \quad \text{(B2)}$$

where $X = (\alpha/\chi)Q' + \rho(YQ'' + Y'Q')$. Eliminating X, we arrive at

$$\frac{\Delta}{1+\kappa^2}\left(\frac{\alpha}{\chi}+\rho Y'\right)Y + \frac{\Delta}{1+\kappa^2}\frac{\alpha\omega}{\chi}\left(1+\frac{\omega_c}{\omega}\sin 2\psi\right) = cY(1+\kappa^2)\left(\frac{\kappa\Delta}{1+\kappa^2}-Q'\right)\cos\psi. \quad \text{(B3)}$$

We assume that

$$Y = -g(\omega+\omega_c)\sin 2\psi, \quad \text{(B4)}$$

where g is a parameter to be determined, then by substituting Eq. (B4) into Eq. (B3), we obtain

$$\frac{\Delta}{1+\kappa^2}\left[2\rho g\omega_c + \left(1-\frac{1}{g}\right)\frac{\alpha}{\chi} - 4\rho g\omega_c\cos^2\psi\right] = c(1+\kappa^2)\left(\frac{\kappa\Delta}{1+\kappa^2}-Q'\right)\cos\psi. \quad \text{(B5)}$$

Since Eq. (B5) is assumed to hold for every ψ, the coefficients of powers of $\cos\psi$ must balance and we obtain

$$2\rho g\omega_c + \left(1-\frac{1}{g}\right)\frac{\alpha}{\chi} = 0, \quad \text{(B6a)}$$

$$-4g\frac{\Delta}{1+\kappa^2}\rho\omega_c\cos\psi = c(1+\kappa^2)\left(\frac{\kappa\Delta}{1+\kappa^2}-Q'\right). \quad \text{(B6b)}$$

The coefficient g can be determined from Eq. (B6a), which gives

$$g = (\sqrt{1+8\rho\omega_c\chi/\alpha}-1)\alpha/(4\rho\chi\omega_c). \quad \text{(B7)}$$

Equation (B6b) results in

$$Q' = \frac{\Delta}{1+\kappa^2}\left(\kappa + 4g\rho\frac{d}{c}\frac{\chi}{\alpha}\cos\psi\right) \quad \text{(B8)}$$

and thus we have $\langle Q'\rangle = \kappa\Delta/(1+\kappa^2)$.

[1] E. V. Gomonay and V. M. Loktev, Low Temp. Phys. **40**, 17 (2014).

[2] R. Cheng, J. Xiao, Q. Niu, and A. Brataas, Phys. Rev. Lett. **113**, 057601 (2014).

[3] T. Jungwirth, X. Marti, P. Wadley, and J. Wunderlich, Nat. Nanotechnol. **11**, 231 (2016).

[4] P. Wadley *et al.*, Science **351**, 587 (2016).

[5] E. G. Tveten, A. Qaiumzadeh, O. A. Tretiakov, and A. Brataas, Phys. Rev. Lett. **110**, 127208 (2013).

[6] O. Gomonay, T. Jungwirth, and J. Sinova, Phys. Rev. Lett. **117**, 017202 (2016).

[7] T. Shiino, S.-H. H. Oh, P. M. Haney, S.-W. W. Lee, G. Go, B.-G. G. Park, and K.-J. J. Lee, Phys. Rev. Lett. **117**, 087203 (2016).

[8] R. Cheng, M. W. Daniels, J.-G. Zhu, and D. Xiao, Sci. Rep. **6**, 24223 (2016).

[9] J. Lan, W. Yu, and J. Xiao, Nat. Commun. **8**, 178 (2017).

[10] H. Y. Yuan and X. R. Wang, Appl. Phys. Lett. **110**, 082403 (2017).

[11] W. Wang, C. Gu, Y. Zhou, and H. Fangohr, Phys. Rev. B **96**, 024430 (2017).

[12] B. Hillebrands and A. Thiaville, *Spin Dynamics in Confined Magnetic Structures III* (Springer, New York, 2006).

[13] E. G. Tveten, A. Qaiumzadeh, and A. Brataas, Phys. Rev. Lett. **112**, 147204 (2014).
[14] A. Qaiumzadeh, L. A. Kristiansen, and A. Brataas, Phys. Rev. B **97**, 020402 (2018).
[15] W. Yu, J. Lan, and J. Xiao, arXiv:1711.08929.
[16] E. G. Tveten, T. Müller, J. Linder, and A. Brataas, Phys. Rev. B **93**, 104408 (2016).
[17] H. Y. Yuan, W. Wang, M.-H. Yung, and X. R. Wang, arXiv:1712.03055.
[18] S. Selzer, U. Atxitia, U. Ritzmann, D. Hinzke, and U. Nowak, Phys. Rev. Lett. **117**, 107201 (2016).
[19] P. Yan and X. R. Wang, Phys. Rev. B **80**, 214426 (2009).
[20] F. D. M. Haldane, Phys. Rev. Lett. **50**, 1153 (1983).
[21] R. Article and A. K. Ghosh, Eur. Phys. J. B **82**, 19 (2011).
[22] T. Kampfrath, A. Sell, G. Klatt, A. Pashkin, S. Mährlein, T. Dekorsy, M. Wolf, M. Fiebig, A. Leitenstorfer, and R. Huber, Nat. Photonics **5**, 31 (2011).
[23] N. Papanicolaou, Phys. Rev. B **55**, 12290 (1997).
[24] K. M. D. Hals, Y. Tserkovnyak, and A. Brataas, Phys. Rev. Lett. **106**, 107206 (2011).
[25] Q. Liu, H. Y. Yuan, K. Xia, and Z. Yuan, Phys. Rev. Mater. **1**, 061401 (2017).
[26] W. Wang, M. Albert, M. Beg, M.-A. Bisotti, D. Chernyshenko, D. Cortés-Ortuño, I. Hawke, and H. Fangohr, Phys. Rev. Lett. **114**, 087203 (2015).
[27] P. Yan and G. E. W. Bauer, Phys. Rev. Lett. **109**, 087202 (2012).
[28] T. Taniguchi, Phys. Rev. B **90**, 024424 (2014).
[29] S. J. Pickart, M. F. Collins, and C. G. Windsor, J. Appl. Phys. **37**, 1054 (1966).
[30] D. J. Lockwood and G. J. Coombs, J. Phys. C: Solid State Phys. **8**, 4062 (1975).
[31] J. Barker and O. A. Tretiakov, Phys. Rev. Lett. **116**, 147203 (2016).